Inequality of avalanche sizes in models of fracture

Diksha,[1] Sumanta Kundu,[2,3] Bikas K. Chakrabarti,[4] and Soumyajyoti Biswas[1]
[1]*Department of Physics, SRM University-AP, Andhra Pradesh 522240, India*
[2]*Department of Physics and Astronomy, University of Padova, Via Marzolo 8, I-35131 Padua, Italy*
[3]*INFN, Sezione di Padova, Via Marzolo 8, I-35131 Padua, Italy*
[4]*Saha Institute of Nuclear Physics, 1/AF Bidhannagar, Kolkata 700064, India*

(Received 21 March 2023; accepted 13 June 2023; published 5 July 2023)

Prediction of an imminent catastrophic event in a driven disordered system is of paramount importance—from the laboratory scale controlled fracture experiment to the largest scale of mechanical failure, i.e., earthquakes. It has long been conjectured that the statistical regularities in the energy emission time series mirror the "health" of such driven systems and hence have the potential for forecasting imminent catastrophe. Among other statistical regularities, a measure of how unequal avalanche sizes are is potentially a crucial indicator of imminent failure. The inequalities of avalanche sizes are quantified using inequality indices traditionally used in socioeconomic systems: the Gini index g, the Hirsch index h, and the Kolkata index k. It is shown analytically (for the mean-field case) and numerically (for the non-mean-field case) with models of quasi-brittle materials that the indices show universal behavior near the breaking points in such models and hence could serve as indicators of imminent breakdown of stressed disordered systems.

DOI: 10.1103/PhysRevE.108.014103

I. INTRODUCTION

When a solid is slowly loaded to its breaking point, it goes through many instances of microscopic damage. Such microscopic damage can grow with additional applied load, interact via the stress field modification, and accumulate into a macroscopic failure (for example, a shear plane in the case of compression induced damage in quasi-brittle objects). However, all breaking events are not equally damaging. Indeed, if we go by the acoustic energy signal S emitted in each event, the size distribution of these signals $P(S)$ usually has a fat tail [$P(S) \sim S^{-\delta}$], implying a very small number of events account for most of the damage incurred [1,2]. This "damage inequality" is reminiscent of inequalities observed in myriad complex systems, including physical (from crackling noise [3] in magnetic domain wall movements to the largest mechanical failures during earthquakes [4]), sociological [5] (deaths in armed conflicts, citations of papers), and economic (wealth distribution) [6] systems. This fat-tail or power-law behavior is often attributed to a critical point in the system that is reached either through the fine tuning of an external parameter or the system self-organizing to the critical point through a slow drive [7].

It was empirically noted by Pareto in 1896 in his famous 80-20 law that 80% of wealth is accumulated by 20% of the richest people. Since then, this observation was much broadly applied, showing that in many socioeconomic systems 80% of "successes" come from 20% of "attempts" [8]. Since then, much has been achieved in studies on inequality, primarily in socioeconomic systems, mostly because of the immense adverse effect such inequalities could have in socioeconomic contexts [9]. A very recent interest is to understand inequality in the responses of physical systems, particularly when such systems are near a critical point [10]. The main goal in such a scenario is to forecast imminent catastrophe (or distance to the critical point) in such systems. For example, it was shown that in models of fracture, the growing inequality of avalanche sizes shows universal behavior near the critical point [10]. It was then shown that with a supervised machine learning algorithm, measures of inequality of avalanche sizes were the most important attribute for predicting the imminent failure point [11] in models of quasi-brittle materials. It was also shown subsequently that a family of self-organized critical (SOC) systems (e.g., Bak-Tang-Wiesenfeld and Manna sandpile models, among others) also show universal behavior in terms of the inequality measures of their responses (avalanches) [12]. Along those lines, extensive data analysis showed that in a wide variety of socioeconomic systems that have been conjectured to be in self-organized critical states, the measures of inequalities in such systems exhibit behavior similar to that seen in SOC models. Such observations underline the importance of the inequality measures of responses of a system near its critical point for uncovering the formal link between such measures and critical phenomena [13] and also to make use of such a link for the practical purposes of forecasting an imminent critical point in systems where such a point could have a catastrophic consequence (for example, in fractures and earthquakes).

In this work, we study two generic models of fracture in disordered quasi-brittle solids, the fiber bundle model (FBM) and the random fuse model (RFM), in terms of the inequality of their response functions (avalanche time series) as they are stressed to their breaking points. Particularly, in the mean-field FBM, we analytically calculate the inequality indices and their scaling behavior near the critical point, thereby illustrating the previously numerically observed universal behavior. We also study the more realistic non-mean-field limit of the FBM and the RFM and show numerically that similar scalings

are observed (with different exponent values) in such cases as well.

This paper is organized as follows: first, we define the indices that were used to quantify the inequalities in the avalanche statistics of these models; then we describe the models and their simulations. We then go on to present the analytical calculations for the mean-field case and compare them with previous numerical studies. Then we give the numerical results for the non-mean-field case of the FBM and the RFM. Finally, we discuss the results and their implications for forecasting imminent failure in these models and potentially in experiments and conclude.

II. QUANTIFICATION OF THE INEQUALITY OF AVALANCHES: THE INEQUALITY INDICES

Inequalities in socioeconomic contexts have been quantified using several indices, for example, the Gini index g [14] (for wealth), the Hirsch index h (for citations) [15], and, more recently, the Kolkata index k [16]. The role of these indices in parametrizing socioeconomic inequality has expanded over the past few decades. These inequality measures are defined through the Lorenz curve. When a time series is arranged in ascending order of the size of the values in the series, the Lorenz function $L(p)$ gives the cumulative fraction of the total "mass" acquired by the p fraction of the smallest events. If all the values are equal in size, then the Lorenz function will be a diagonal line from the origin to (1,1), known as the equality line. But, in general, these values are not equal in size, so the Lorenz function is nonlinear, always staying under the equality line and increasing monotonically from $L(p=0)=0$ to $L(p=1)=1$. The Gini index is then given by twice the area between the Lorenz curve and the equality line, where $g=0$ implies perfect equality and $g=1$ indicates extreme inequality. The crossing point of the opposite diagonal line with the Lorenz curve gives the value of the Kolkata index k, which says that the $(1-k)$ fraction of the largest events accounts for the k fraction of the total events, where $k=0.5$ indicates perfect equality and $k=1$ represents extreme inequality. The Hirsch index is generally calculated in the case of citations of individual scientists or scholars, but the definition can be expanded to measure the h-index of any series. The h-index is then the highest number h such that h events each have at least a size of h. For a more detailed discussion on the definitions of these measures, see Ref. [13].

In this work, we will measure the inequality of the time series of avalanches recorded for slowly loaded disordered materials, represented by generic threshold activated models. Therefore, for our purposes, the Lorenz function $L(p)$ represents the fraction of the breaking events resulting from the smallest p fraction of avalanches. The other definitions follow the same line. We will show how the inequalities grow as the system gradually approaches the catastrophic failure points. Most importantly, we will monitor the values g_f, k_f, and h_f that the inequality indices take just prior to the catastrophic breakdown. We are interested in the universality of these values and also the finite size and off-critical scaling behavior these measures show, particularly in the context relevant to forecasting an imminent failure.

III. MODELS AND METHODS

As mentioned before, in this work we consider two generic models of fracture: the fiber bundle model [17,18] and the random fuse model [19–21]. In the FBM, an ensemble of N linear elastic fibers which have different individual breaking thresholds is considered. When a load is applied to all the fibers, some of the weak fibers fail, and the load carried by those fibers is redistributed among the remaining ones, which might in turn fail, leading to an avalanche event. At a critical value of the load, the entire system collapses. In the RFM, an ensemble of electrical fuses is arranged in a network (say, a square lattice). Each fuse has a failure threshold, beyond which it burns out. When a voltage difference is applied across the system (say, the two ends of a square lattice), the weaker fuses are burned out, requiring the current to be diverted through other paths, which might in turn cause other fuses to burn out, leading to an avalanche event. The modification in the flow of current due to burnt-out fuses mimics the modification of the stress field in an elastic solid due to local damage. Both of these models have been very well studied in the literature from various viewpoints of applications of fracture in disordered systems [22,23] and mimic many experimentally observed features, such as power-law scaling of avalanches (see, e.g., [2]) and nonlinear stress-strain relations (see, e.g., [24]).

Finding an indication of the imminent failure in these models without using detailed information regarding the individual failure thresholds is therefore a long-standing crucial issue. This problem has been approached in various different ways, including changes in the avalanche size distribution exponent prior to failure [25] and nonmonotonic behavior of the elastic energy stored in the system [26]. However, here we study the behavior of the inequality indices, which have shown promising indications as precursory measures of imminent breakdown [11].

A. Simulation methods

While a mean-field limit of the FBM is analytically tractable, more realistic versions of the FBM and also the RFM are not. Those limits are accessed through numerical simulations. Therefore, here we describe the simulation methods for the two models, with which the avalanche time series could be obtained. The inequality indices are then measured using those time series. The codes used to produce the simulation results are available in Ref. [27].

1. Simulating FBM

In the FBM, a large number of parallel fibers are connected between two horizontal plates. The top plate with hanging fibers is rigid, and the rigidity of the lower plate determines the interaction range of the model. All the fibers are assumed here to have identical elastic constants but have different failure thresholds. Here the failure thresholds of the fibers are randomly assigned from a uniform distribution between 0 and 1. When a load is applied to the system, the weakest fibers fail irreversibly, and the load of the broken fibers is redistributed to the remaining intact fibers. The increased load on the surviving fibers then may cause more failures, and this process will

go on until the remaining fibers are strong enough to hold the extra load or the whole bundle collapses. The external load is kept constant throughout the redistribution process, and then it is increased to initiate the dynamics again after the dynamics stops. The number of fibers breaking between two successive load increments is called an avalanche. The redistribution of the load mentioned above depends on the elastic properties of the lower plate. The two cases of load redistribution are equal load sharing (ELS) and local load sharing (LLS). In ELS, when the lower plate is absolutely rigid, the load of the broken fiber is equally redistributed among all surviving fibers; hence, it is the mean-field limit. In LLS, when the lower plate deforms under loading, a higher fraction of the load of the broken fiber is carried by the surviving neighbors that are closer to the broken fiber. The extreme case is nearest neighbor load sharing. But long-range (power-law) load sharing has also been studied before [28]. Here we redistribute the load of the broken fiber between R surviving neighbors on either side (see, e.g., [29]) when the fibers are arranged in a one-dimensional lattice of length L. Clearly, $R = 1$ is the nearest neighbor load sharing, and $R \sim L$ is the ELS limit (in fact, the ELS limit is reached much earlier [30]).

Here we study both the mean-field limit (ELS) and the local load sharing limit with finite values of R. We mention the respective cases in the results as appropriate.

2. Simulating RFM

The random fuse network model that we consider here is defined on a two-dimensional tilted square lattice of linear size L with periodic boundary conditions along the horizontal direction. A potential difference is applied along the vertical direction between the two opposite sides of the lattice. Each bond i representing an Ohmic resistor with unit conductance carries electrical current i_i until it burns out irreversibly at a threshold value b_i of its current, and then it becomes an insulator. The thresholds values $\{b_i\}$ are selected randomly and independently from a power-law distribution: $p(b) \sim b^{-1}$, bounded between $10^{-\beta}$ and 10^{β}. This is a generic form of distribution with a decaying power-law tail that has been considered widely for modeling fractures of heterogeneous materials with varying degrees of disorder [29,31–33].

Initially, all the bonds are intact, and the applied voltage difference V is raised quasi-statically from zero. The specific geometry of our lattice ensures that every bond initially carries the same amount of current. Therefore, the breaking process initiates when the current through the "weakest bond" in the system reaches its breaking threshold at $V = V_0 = (L-1) \times \min\{b_i\}$. Subsequently, the bond burns out, and it is irreversibly removed. The new current distribution is then determined by keeping the external voltage difference fixed at $V = V_0$. This may initiate a sequence of bond burning. At this stage, all the bonds carrying currents higher than their respective threshold values are removed simultaneously, and again, the current distribution is calculated. Numerically, to determine the current distribution, a set of Kirchhoff's equations is iteratively solved using the conjugate gradient method with an accuracy of 10^{-12} [34]. The technical details of the method and the convergence criteria that we followed are described in Ref. [34]. In this way, the breaking process continues until a stable state is reached when the current through all the remaining intact bonds is lower than their respective breaking thresholds. This completes an avalanche. The largest ratio between the current and threshold, i.e., $\max(i_i/b_i)$, is then calculated for all intact bonds i to determine the next weakest bond to be burned out and removed. This initiates a new avalanche. Accordingly, the external voltage difference is raised.

In this voltage-controlled setting, the breaking process stops completely when a final crack comprising burnt-out bonds wraps around the lattice in a direction transverse to the applied potential difference; that is, no current flows through the system. The number of bonds that burn out between two successive increments of the external voltage determines the avalanche size.

Note that at an early stage of the breaking process, the intact bond with the minimum value of the breaking threshold determines the weakest bond. However, depending on the value of β, this is not generally true at the later stage. The current concentration around the crack zone competes with the local strength of the breaking thresholds. As a consequence, the breaking events become correlated [21,31,35,36]. Certainly, the choice of β is important, as discussed in Ref. [31]. In the limit of weak disorder, i.e., $\beta \to 0$, the width of the distribution is so narrow that the fracture process becomes localized and only a single crack grows in the system, while it becomes percolation-like in the limit of strong disorder, i.e., $\beta \to \infty$. In the latter case, one gets only avalanches of size unity and always burns out the intact bond with the smallest breaking threshold on the conducting backbone. Importantly, depending on L, the breaking dynamics is avalanche dominated in the intermediate range of disorder [31,35].

We choose the value of $\beta = 1$ and consider system sizes $L = 32$, 64, 128, 256, and 512 such that the system remains in the transition regime from weak to strong disorder where avalanche dynamics can be observed.

IV. RESULTS

We now move on to describe the behavior of the inequality indices g, h, and k for the avalanche statistics of the FBM and the RFM. We first present the analytical results for the FBM in the mean-field (ELS) limit and then go on to discuss the local load sharing version and the RFM results.

A. Inequality indices for the FBM in the mean-field limit: Analytical results

The FBM in the mean-field (ELS) limit is analytically tractable [18]. The system size (initial number of fibers) is denoted by N, and the applied load is W, making the load per fiber $\sigma = W/N$, with σ_c denoting the critical value at which catastrophic breakdown happens. The fraction of intact fibers at load per fiber σ for a threshold distribution uniform in (0,1) is given by

$$U(\sigma) = U^*(\sigma_c) + (\sigma_c - \sigma)^{1/2}. \tag{1}$$

The magnitude of the change in this fraction for a differential increment in the load per fiber value is therefore

$$S(\sigma) = \left|\frac{dU(\sigma)}{d\sigma}\right| = \frac{1}{2}(\sigma_c - \sigma)^{-1/2}. \tag{2}$$

This is a measure of avalanche size at σ, when the load increment is done by a fixed amount $\Delta = d\sigma$ at every step.

Note that while Eqs. (1) and (2) are written for uniform threshold distribution in (0,1), they are valid, up to a prefactor, for a broad class of threshold distributions [18]. Therefore, all the subsequent results are valid for the same class of threshold distributions. For distributions that are outside this class and can change the failure mode of the bundle from quasi-brittle to an individual fiber breaking dynamics, the inequality estimates for avalanches will also change, as we will see later on.

1. Terminal values of the inequality indices

The function in Eq. (2) is monotonically increasing up to the failure point $\sigma = \sigma_c$; hence, the Lorenz function at the point of collapse of the system is given by

$$L_f(p) = \frac{\int_0^{p\sigma_c} (\sigma_c - \sigma)^{-1/2} d\sigma}{\int_0^{\sigma_c} (\sigma_c - \sigma)^{-1/2} d\sigma}. \tag{3}$$

On simplification, this gives

$$L_f(p) = 1 - \sqrt{1-p}, \tag{4}$$

where σ_c cancels out, giving the function the robustness it shows against various threshold distributions (see Fig. 11 in Ref. [11]). The Gini index g at the point of collapse is then

$$g_f = 1 - 2\int_0^1 L_f(p) dp = \frac{1}{3}. \tag{5}$$

The Kolkata index k at the point of collapse can be found from

$$1 - k_f = L_f(k_f) = 1 - \sqrt{1-k_f}, \tag{6}$$

which gives

$$k_f = \frac{\sqrt{5}-1}{2} \approx 0.618, \tag{7}$$

which is the inverse golden ratio. The other solution is irrelevant.

It is also known [18] that for a fiber bundle model with an equal amount of load increase in each step, the number of fibers broken due to the increase of load between $m\Delta$ and $(m+1)\Delta$ is given by

$$S(m) = \frac{\Delta}{\sqrt{1 - 4m\Delta/N}}, \tag{8}$$

where $m = 0, 1, 2, \ldots, N/4\Delta$. This suggests a monotonic increase in the avalanche size, which is strictly true for equispaced thresholds (given by i/N, $i = 1, \ldots, N$), but the scaling relations are valid for nonequispaced thresholds as well. To find the Hirsch index h, the avalanches should first be sorted in descending order, which we do with the transformation $m \to \frac{N}{4\Delta} - m$, giving

$$S\left(\frac{N}{4\Delta} - m\right) = \frac{\Delta}{\sqrt{1 - \frac{4\Delta}{N}\left(\frac{N}{4\Delta} - m\right)}} = \frac{\Delta}{\sqrt{\frac{4\Delta m}{N}}}. \tag{9}$$

Then the value of the Hirsch index at the point of collapse can be found from

$$\frac{\Delta}{\sqrt{\frac{4\Delta h_f}{N}}} = h_f, \tag{10}$$

which gives

$$h_f \propto N^{1/3}. \tag{11}$$

This scaling is in contrast to the previously conjectured form (see Ref. [10]). However, as we shall shortly see, this is obeyed in accurate numerical simulations of the model.

2. Off-critical scaling

Now, if the loading is done up to $\sigma = q\sigma_c$, where $q \leqslant 1$, then the Lorenz function can be found from

$$L(p, q) = \frac{\int_0^{pq\sigma_c} (\sigma_c - \sigma)^{-1/2} d\sigma}{\int_0^{q\sigma_c} (\sigma_c - \sigma)^{-1/2} d\sigma}, \tag{12}$$

which gives

$$L(p, q) = \frac{1 - \sqrt{1-pq}}{1 - \sqrt{1-q}}, \tag{13}$$

which, in the limit $q = 1$, gives L_f in Eq. (4). It is then possible to calculate the evolution of g and k as the load is increased using

$$g(q) = 1 - 2\int_0^1 L(p, q) dp, \tag{14}$$

which gives, on simplification,

$$g = 1 - \frac{4(1-q)\sqrt{1-q} + 6q - 4}{3q(1 - \sqrt{1-q})}. \tag{15}$$

Similarly, the equation for $k(q)$ reads

$$k(q) = 1 - \frac{1 - \sqrt{1 - k(q)q}}{1 - \sqrt{1-q}}. \tag{16}$$

For any value of q, the value of $k(q)$ can be numerically estimated with arbitrary accuracy from the equation above. In Fig. 1, the values obtained for $k(q)$ from the above equation are plotted against those obtained for $g(q)$ from Eq. (16). The phenomenologically derived expression $k = \frac{1}{2} + \frac{3}{8}g$ [13] is also plotted for reference. Furthermore, simulation results for two threshold distributions, uniform in (0,1) and Weibull (with a shape parameter value of 1.3), are also shown. For lower values of g, for which the phenomenological argument is valid, the two expressions match. For higher values of g, the simulations follow the analytical estimate. Given that g and k are almost linearly related, for the subsequent part of this work, we keep the focus on calculating g, which can be done in closed form. From Eq. (15), the $q \to 1$ limit ($\sigma \to \sigma_c$) yields

$$g - g_f \propto \sqrt{1-q}, \tag{17}$$

meaning that we can write all response functions in terms of the interval $|g - g_f|$ instead of $\sigma - \sigma_c$ with the appropriate changes in the scaling exponent (see Ref. [37] for details). An important consequence of the above equation is the finite size scaling of the terminal value of g. We can define a correlation length exponent as $\xi \propto |\sigma - \sigma_c|^{-\nu}$ [38], which will span the system size at the critical point. We should then have, for a finite size system at its critical point, $|\sigma_c(N) - \sigma_c(N \to \infty)| \propto N^{-1/\nu}$. Also, at the critical point of the finite system,

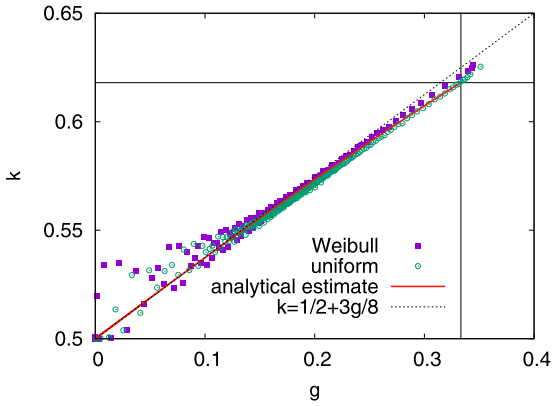

FIG. 1. The plot of $k(q)$ [obtained numerically from Eq. (16)] against $g(q)$ [obtained from Eq. (15)] for the mean-field FBM. The numerical simulations are also shown for two threshold distributions: uniform and Weibull. The line $k = \frac{1}{2} + \frac{3}{8}g$ is plotted for reference and matches well the analytical estimate for small values of g. The failure point values of g and k, given by $g_f = 1/3$ [see Eq. (5)] and $k_f = (\sqrt{5}-1)/2 \approx 0.618$ [see Eq. (7)], are indicated by a vertical line and a horizontal line, respectively. These results indicate that the values of k and g are universal for a broad class of threshold distributions.

we should have, from Eq. (17),

$$g_f(N) - g_f(N \to \infty) \propto |\sigma_c(N) - \sigma_c(N \to \infty)|^{1/2} \propto N^{-1/2\nu}. \tag{18}$$

Given that $\nu = 3/2$ [32,38], we should have $|g_f(N) - g_f(N \to \infty)| \propto N^{-1/3}$, which is what we see in Fig. 2.

To find the load and size dependence of h, consider again Eq. (8). Suppose we stop the loading at $m = m_{\max} = \frac{qN}{4\Delta}$, where $q \leqslant 1$, as before. The avalanches arranged in descending order would then read

$$S(m_{\max} - m) = \frac{\Delta}{\sqrt{1 - \frac{4\Delta}{N}(m_{\max} - m)}} = \frac{\Delta}{\sqrt{1 - \frac{4\Delta}{N}\left(\frac{qN}{4\Delta} - m\right)}}. \tag{19}$$

The Hirsch index can then be found, as before, from

$$\frac{\Delta}{\sqrt{1 - \frac{4\Delta}{N}\left(\frac{qN}{4\Delta} - h\right)}} = h. \tag{20}$$

This can be simplified to

$$h^3 + \frac{N(1-q)}{4\Delta}h^2 - \frac{N\Delta}{4} = 0. \tag{21}$$

This cubic equation can be solved (see the Appendix). But the expression for h is then too complex to figure out the scaling form near the critical point. Instead, we can approximate that near the critical point ($q \to 1$), the cubic term in h will be the most dominant and hence be responsible for the leading order scaling. In that case, the quadratic term can be replaced by its value exactly at the critical point, $h_f^2 = (\frac{\Delta N}{4})^{2/3}$. Then, near the critical point $\sigma_c = 1/4$,

$$\frac{4\Delta}{N}h^3 \approx \Delta^2 - (1-q)\left(\frac{\Delta N}{4}\right)^{2/3}. \tag{22}$$

This gives

$$h^3 \approx \frac{N\Delta}{4} - \frac{1-q}{4}\frac{N}{\Delta}\left(\frac{\Delta N}{4}\right)^{2/3}. \tag{23}$$

On simplification, this gives

$$h^3 \approx \frac{\Delta N}{4} - \frac{1-q}{4}\frac{N}{\Delta}\left(\frac{\Delta N}{4}\right)^{2/3} \approx N\left[\frac{\Delta}{4} - (\sigma_c - \sigma)N^{2/3}\left(\frac{1}{4\sqrt{\Delta}}\right)^{2/3}\right], \tag{24}$$

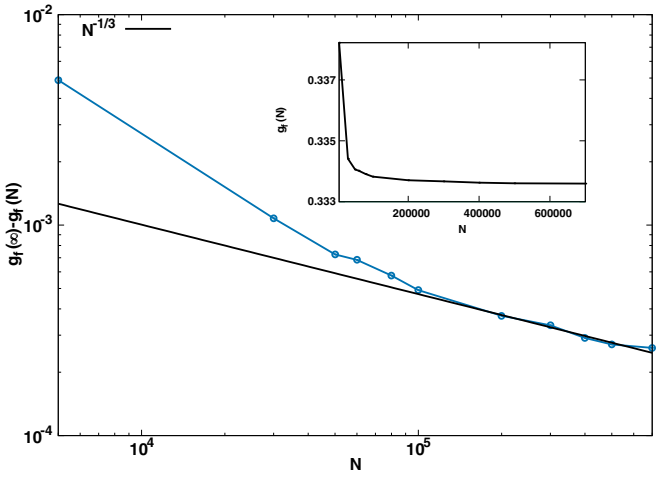

FIG. 2. Finite-size scaling of g for different system sizes ($N/10^3 = 5$, 30, 50, 60, 80, 100, 200, 300, 400, 500, 700) for the mean-field fiber bundle model. From this plot, we can see that g_f shows the finite size scaling mentioned in Eq. (18) in the limit of large system sizes. The inset shows the variation of $g_f(N)$ with system size (N).

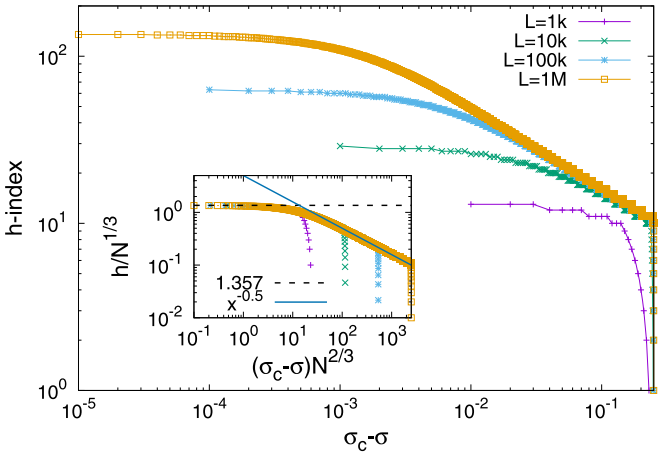

FIG. 3. The finite size scaling of the h-index, following Eqs. (22) and (23) for the mean-field FBM. In the inset, the limiting behavior of the scaled function is also indicated; it saturates to $(5/2)^{1/3}$ with loading step size $\Delta = 10$ for small values of the argument and decays as a power law with an exponent of $-1/2$ for large values of the argument (see text).

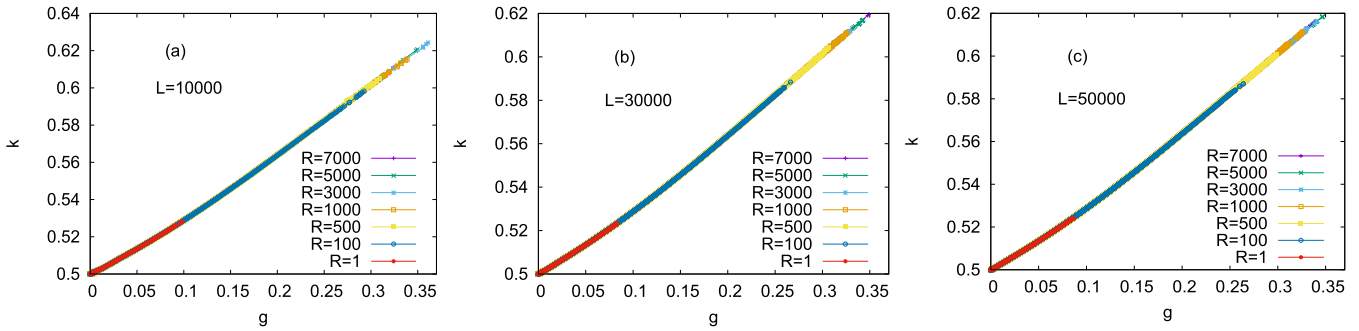

FIG. 4. Plot of $g(q)$ against $k(q)$ for different interaction ranges ($R = 1, 100, 500, 1000, 3000, 5000, 7000$) for three different system sizes ($L = 10\,000, 30\,000, 50\,000$) in the LLS fiber bundle model. The plot shows that terminal values of g and k are independent of the system sizes. With an increasing value of R, the terminal values of g and k approach the values obtained analytically in the mean-field limit.

where $\frac{1-q}{4} = \sigma_c - \sigma$ (recalling that $\sigma = q\sigma_c$). This is now in the scaling form

$$h \approx N^{1/3} f[(\sigma_c - \sigma)N^{1/\nu}], \tag{25}$$

with $\nu = 3/2$ [32] being the correlation length exponent.

Figure 3 shows the numerical validation of the scaling form above. The simulation was done for a fixed load increase with $\Delta = 10$. So, as $\sigma \to \sigma_c$, the quantity $h/N^{1/3}$ should tend to $(5/2)^{1/3} \approx 1.357$, which it does (as can be seen from the inset of Fig. 3). Also, away from the critical point, the quantity should be proportional to $(\sigma_c - \sigma)^{-1/2}$, which is also seen. The data collapse for the three orders of magnitude system size variation confirms the scaling $h_f \sim N^{1/3}$.

B. Inequality indices in the non-mean-field limit of the FBM: Simulation results

This is the case in which the load of a broken fiber is redistributed to the nearest R surviving fibers when they are arranged in a one-dimensional lattice of size L. Here we take the threshold distribution to be uniform between 0 and 1. Here $R = 1$ means that the sharing of the load is fully local. In this case, we take three different system sizes ($L = 10\,000, 30\,000, 50\,000$) and vary the value of R and then calculate the values of h, g, and k. In Fig. 4 we plot g against k, and we observe numerically that when the interaction range R is increased, the g_f and k_f values are very close to the analytical results obtained for the mean-field case. Prior to reaching the terminal values, the variation of g vs k almost follows the mean-field variation, except that the growth stops earlier (usually, there are fewer avalanches for local load sharing). In Fig. 5 the variation of h is plotted for different values of R. Here also, the terminal values are smaller for lower values of R, and so is their system size scaling. Indeed, from Fig. 6 it can be seen that for fully local load sharing ($R = 1$), scaling of h_f shows logarithmic dependence on L, but as we increase the interaction range, the scaling of h_f shows power-law dependence on $L^{1/3}$, similar to what we expect in the mean-field limit.

C. Inequality indices for the RFM: Simulation results

Finally, we compare the above results with a more realistic model of fracture, the RFM on a tilted square lattice. In this case, the threshold distribution is a power law with an exponent of -1, as mentioned before. The limits of the distribution are between $10^{-\beta}$ and 10^{β}. We choose the value of $\beta = 1$ for system sizes $L = 32, 64, 128, 256$, and 512. We calculated the inequality measures using 500 samples for system sizes up to $L = 256$ and 40 samples for $L = 512$. Given that $N = L \times L$, if we expect a scaling similar to that in the case of the FBM, we should have $h_f \sim L^{2/3}$ (since $N = L \times L$ here). In Fig. 7, the function $h/L^{2/3}$ collapses on a single curve, indicating scaling similar to that in the FBM.

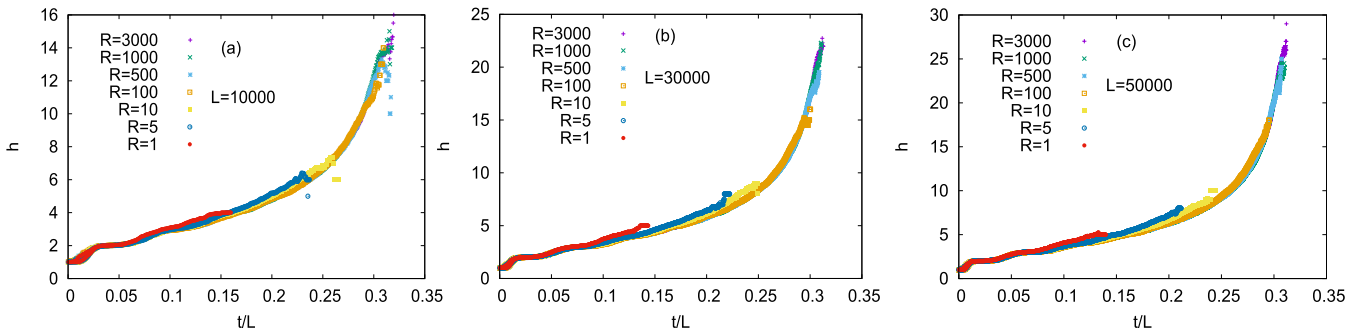

FIG. 5. The variation of the h-index with rescaled time t/L for different interaction ranges ($R = 1, 5, 10, 500, 1000, 3000$) for three different system sizes ($L = 10\,000, 30\,000, 50\,000$) for the LLS fiber bundle model.

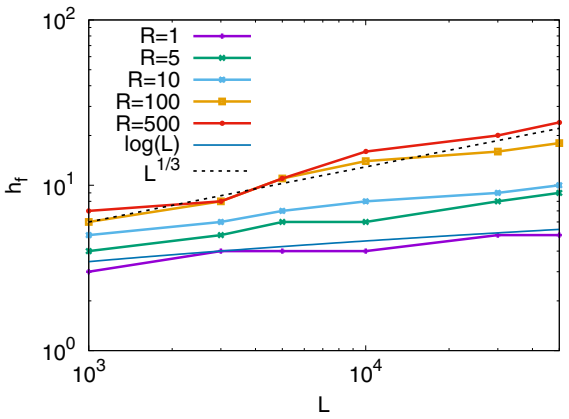

FIG. 6. System size L dependence of the terminal values of $h = h_f$ for different interaction ranges R for the one-dimensional LLS fiber bundle model in a log-log scale. It is seen that for $R = 1$, when the load sharing is fully local, h_f shows a logarithmic dependence, and when $R = 100$ and 500, h_f shows the power-law dependence. Here the solid (blue) and dashed (black) lines indicate the $\log(L)$ and $L^{1/3}$ functional form, respectively.

The values of g_f and k_f are set by the avalanche size distribution exponent. Particularly, if the avalanche size distribution exponent is δ, then it is straightforward to see that when the avalanches are arranged in ascending order of their sizes, the resulting curve will diverge with an exponent $n = 1/(\delta - 1)$. For $\beta = 1.0$, $\delta \approx 1.99$. Now, it is also possible to show [37] that for $n > 1$, $g_f = k_f = 1$. Therefore, in the finite size scaling of their values, we would have to set $g_f(L \to \infty) \to 1$, resulting in a scaling form as before $|1 - g_f(L)| \propto L^{-1/2\nu}$. In Fig. 8, we do see a power-law decay of $|1 - g_f(L)|$ with L, but not with the expected exponent value (typically, $\nu = 4/3$ for the RFM [39]). Nevertheless, the power-law scaling is seen, with an exponent of -0.23.

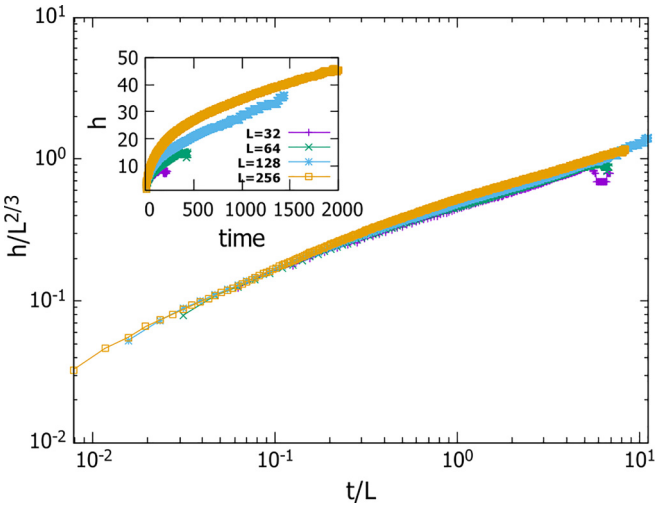

FIG. 7. The h-index (scaled by $L^{2/3}$) is plotted against the time (scaled by time/L) for different system sizes ($L = 32, 64, 128, 256$) for the two-dimensional random fuse model with a power-law distributed breaking threshold. The inset shows the variation of h with time for the different system sizes.

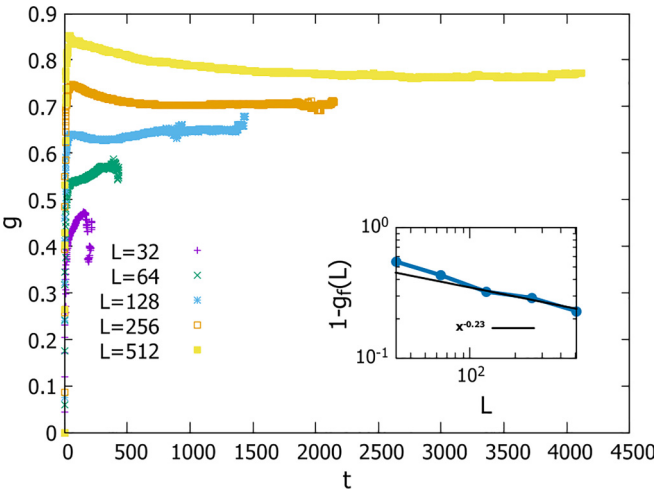

FIG. 8. The g-index is plotted against time for different system sizes ($L = 32, 64, 128, 256, 512$) for the random fuse model with a power-law distributed breaking threshold. As can be seen, the terminal values of g change with the system size. The inset shows the variation of the terminal values of the g-index with time in the log-log scale, exhibiting a power-law scaling.

V. DISCUSSION AND CONCLUSION

Near a critical point, the responses of a system show critical divergence. This necessarily means that the responses are highly unequal as a critical point is gradually approached. In the case of disordered solids and their models, these unequal responses are observed in terms of the avalanche time series, which are accumulated local breaking events, experimentally detected as acoustic emissions. It is well known that the statistical properties of such acoustic emissions are useful for characterizing the "health" of a system, i.e., estimating the vicinity of an approaching critical (breaking) point.

Recently, quantitative measures of the inequality of such avalanches, e.g., the Hirsch index h, the Gini index g, and the Kolkata index k, were used to forecast the imminent critical point in physical systems [10]. Particularly, it was noted that g and k reach universal terminal values g_f and k_f at the critical point, irrespective of the details of the system (types of disorder present in them). It is therefore very useful to monitor the inequality of the avalanche statistics to estimate the distance from an approaching critical point [11]. It is more useful to monitor the inequality indices than other universal quantities, e.g., the avalanche size distribution critical exponent, because such an exponent shows universal properties only in the asymptotic limit of large avalanche sizes, where failure is already extremely imminent. Indeed, extensive numerical simulations and machine learning studies have indicated the same thing [11]. This means that for experimental measurements, inequalities of the acoustic emissions, not just their sizes, could play an important role in the indication of an approaching failure point.

Here we showed analytically, in the mean-field FBM, the scaling behavior of the critical indices (h, k, and g). Particularly, for the terminal values of the inequality indices we showed that $h_f \sim N^{1/3}$, where N is the system size,

$g_f = 1/3$, and $k_f = (\sqrt{5}-1)/2$. We also showed the off-critical Widom-Stauffer-like scaling for h [see Eq. (25)]. These were also verified numerically (see Figs. 3 and 6). Some of these scaling relations differ from what was conjectured using only numerical simulations before [10].

We then studied the more realistic local load sharing non-mean-field version of the FBM and also the RFM. In the LLS-FBM, we saw that the scaling of h_f shifts from a logarithmic dependence for very localized load sharing to the power-law dependence mentioned above as the load sharing range R is increased. However, the power-law scaling with system size was observed for the RFM (see Fig. 7). We also showed the finite size effect in g_f for the FBM and the RFM (see Figs. 2 and 8).

In conclusion, the inequalities of the avalanche sizes in models of fracture show universal scaling properties near the failure point. Here we showed analytically (for the mean-field FBM) and numerically (for the non-mean-field FBM and RFM) the scaling properties of the inequality indices. These results show that monitoring the inequality indices in stressed disordered solids can indicate when a critical point is being approached, as was conjectured from numerical and machine learning analysis before.

ACKNOWLEDGMENTS

S.K. is supported by the Research Grant No. ORLA_BIRD2020_01 from the University of Padova. B.K.C. is grateful to the Indian National Science Academy for their Senior Scientist Research Grant. The simulations of the FBM were done using HPCC Surya at SRM University-AP.

APPENDIX: THE EXACT SOLUTION FOR h

As mentioned before, a full solution of Eq. (21) is possible [40]. The equation can be compared with the general cubic form $ah^3 + bh^2 + ch + d = 0$, with $a = 1$, $b = \frac{N(1-q)}{4\Delta}$, $c = 0$, and $d = -\frac{N\Delta}{4}$. Let us now define the quantities $D_0 = b^2 - 3ac = \frac{N^2(1-q)^2}{16\Delta^2}$ and $D_1 = 2b^3 - 9abc + 27a^2d = \frac{N^3(1-q)^3}{32\Delta^3} - \frac{27N\Delta}{4}$. Then we consider $C = \sqrt[3]{\frac{D_1 \pm \sqrt{D_1^2 - 4D_0^3}}{2}}$.

Finally, the three roots are

$$h = -\frac{1}{3}\left(\frac{N(1-q)}{4\Delta} + \zeta^m C + \frac{D_0}{\zeta^m C}\right), \tag{A1}$$

with $m \in \{1, 2, 3\}$ and $\zeta = \frac{-1+\sqrt{-3}}{2}$. Of course, only the real root will be physically meaningful.

[1] S. Biswas, P. Ray, and B. K. Chakrabarti, *Statistical Physics of Fracture, Breakdown and Earthquake* (Wiley, Hoboken, NJ, 2015).

[2] D. Bonamy and E. Bouchaud, Failure of heterogeneous materials: A dynamic phase transition? Phys. Rep. **498**, 1 (2011).

[3] J. P. Sethna, K. A. Dahmen, and C. R. Myers, Crackling noise, Nature (London) **410**, 242 (2001).

[4] B. Gutenberg and C. F. Richter, *Seismicity of the Earth and Associated Phenomena* (Princeton University Press, Princeton, NJ, 1949), p. 295.

[5] A. Chatterjee, A. Ghosh, J. Inoue, and B. K. Chakrabarti, Social inequality: From data to statistical physics modeling, J. Phys.: Conf. Ser. **638**, 012014 (2015).

[6] B. K. Chakrabarti, A. Chakraborti, S. R. Chakravarty, and A. Chatterjee, *Econophysics of Income and Wealth Distributions* (Cambridge University Press, Cambridge, 2013).

[7] P. Bak, C. Tang, and K. Wiesenfeld, Self-Organized Criticality: An Explanation of the $1/f$ Noise, Phys. Rev. Lett. **59**, 381 (1987).

[8] V. Pareto, Cours d' economie politique (1896), reprinted in *Œuvres Complètes* (Droz, Geneva, 1964), Vol. 1.

[9] F. Bourguignon, *Globalization of Inequality* (Princeton University Press, Princeton, NJ, 2015).

[10] S. Biswas and B. K. Chakrabarti, Social inequality analysis of fiber bundle model statistics and prediction of materials failure, Phys. Rev. E **104**, 044308 (2021).

[11] Diksha and S. Biswas, Prediction of imminent failure using supervised learning in a fiber bundle model, Phys. Rev. E **106**, 025003 (2022).

[12] S. S. Manna, S. Biswas, and B. K. Chakrabarti, Near universal values of social inequality indices in self-organized critical models, Physica A (Amsterdam, Neth.) **596**, 127121 (2022).

[13] A. Ghosh, S. Biswas, and B. K. Chakrabarti, Success of social inequality measures in predicting critical or failure points in some models of physical systems, Front. Phys. **10**, 990278 (2022).

[14] H. Dalton, The measurement of the inequality of incomes, Econ. J. **30**, 348 (1920).

[15] J. E. Hirsch, An index to quantify an individual's scientific research output, Proc. Natl. Acad. Sci. USA **102**, 16569 (2005).

[16] A. Ghosh, N. Chattopadhyay, and B. K. Chakrabarti, Inequality in societies, academic institutions and science journals: Gini and k-indices, Physica A (Amsterdam, Neth.) **410**, 30 (2014).

[17] F. T. Pierce, 32—X.—Tensile tests for cotton yarns v.—"The weakest link" theorems on the strength of long and of composite specimens, J. Textile Inst. Trans. **17**, T355 (1926).

[18] S. Pradhan, A. Hansen, and B. K. Chakrabarti, Failure processes in elastic fiber bundles, Rev. Mod. Phys. **82**, 499 (2010).

[19] L. de Arcangelis, S. Redner, and H. J. Herrmann, A random fuse model for breaking processes, J. Phys. Lett. **46**, 585 (1985).

[20] B. Kahng, G. G. Batrouni, S. Redner, L. de Arcangelis, and H. J. Herrmann, Electrical breakdown in a fuse network with random, continuously distributed breaking strengths, Phys. Rev. B **37**, 7625 (1988).

[21] S. Zapperi, P. Ray, H. E. Stanley, and A. Vespignani, First-Order Transition in the Breakdown of Disordered Media, Phys. Rev. Lett. **78**, 1408 (1997).

[22] M. J. Alava, P. K. V. V. Nukala, and S. Zapperi, Statistical models of fracture, Adv. Phys. **55**, 349 (2006).

[23] A. Hansen, P. C. Hemmer, and S. Pradhan, *The Fiber Bundle Model: Modeling Failure in Materials* (Wiley, Hoboken, NJ, 2015).

[24] M. Lebyodkin and T. Lebedkina, On the role of hazard and particle failure statistics on the variation of fracture parameters of ductile-brittle composites, Metals **9**, 633 (2019).
[25] S. Pradhan, A. Hansen, and P. C. Hemmer, Crossover Behavior in Burst Avalanches: Signature of Imminent Failure, Phys. Rev. Lett. **95**, 125501 (2005).
[26] S. Pradhan, J. T. Kjellstadli, and A. Hansen, Variation of elastic energy shows reliable signal of upcoming catastrophic failure, Front. Phys. **7**, 106 (2019).
[27] https://github.com/soumya-84/FBM_RFM.
[28] R. C. Hidalgo, Y. Moreno, F. Kun, and H. J. Herrmann, Fracture model with variable range of interaction, Phys. Rev. E **65**, 046148 (2002).
[29] S. Roy, S. Biswas, and P. Ray, Modes of failure in disordered solids, Phys. Rev. E **96**, 063003 (2017).
[30] S. Roy, S. Biswas, and P. Ray, Failure time in heterogeneous systems, Phys. Rev. Res. **1**, 033047 (2019).
[31] A. A. Moreira, C. L. N. Oliveira, A. Hansen, N. A. M. Araújo, H. J. Herrmann, and J. S. Andrade, Fracturing Highly Disordered Materials, Phys. Rev. Lett. **109**, 255701 (2012).
[32] C. Roy, S. Kundu, and S. S. Manna, Fiber bundle model with highly disordered breaking thresholds, Phys. Rev. E **91**, 032103 (2015).
[33] S. Hope, S. Kundu, C. Roy, S. Manna, and A. Hansen, Network topology of the desert rose, Front. Phys. **3**, 72 (2015).
[34] G. George Batrouni and A. Hansen, Fourier acceleration of iterative processes in disordered systems, J. Stat. Phys. **52**, 747 (1988).
[35] A. Shekhawat, S. Zapperi, and J. P. Sethna, From Damage Percolation to Crack Nucleation through Finite Size Criticality, Phys. Rev. Lett. **110**, 185505 (2013).
[36] A. Hansen and J. Schmittbuhl, Origin of the Universal Roughness Exponent of Brittle Fracture Surfaces: Stress-Weighted Percolation in the Damage Zone, Phys. Rev. Lett. **90**, 045504 (2003).
[37] S. Das and S. Biswas, Critical scaling through Gini-index, arXiv:2211.01281.
[38] S. Biswas and B. K. Chakrabarti, Flory-like statistics of fracture in the fiber bundle model as obtained via Kolmogorov dispersion for turbulence: A conjecture, Phys. Rev. E **102**, 012113 (2020).
[39] T. Ramstad, J. Ø. H. Bakke, J. Bjelland, T. Stranden, and A. Hansen, Correlation length exponent in the three-dimensional fuse network, Phys. Rev. E **70**, 036123 (2004).
[40] Wikipedia, Cubic equation, https://en.wikipedia.org/wiki/Cubic_equation.